IEEE Robotics and Automation Letters (RAL) paper presented at the
2020 IEEE/RSJ International Conference on Intelligent Robots and Systems (IROS)
October 25-29, 2020, Las Vegas, NV, USA (Virtual)

Design, Modelling, and Implementation of a 7-DOF Cable-Driven Haptic Device with a Configurable Cable Platform

Patrice Lambert, Lyndon Da Cruz*, and Christos Bergeles*

***Abstract*— This article introduces a novel 7 Degree Of Freedom (DOF) cable-driven haptic device based on the concept of a configurable cable platform. In the proposed concept, a 1-DOF pinch grasping capability is provided via a network of ten passive cables kept in tension. The coordinated action on the cable platform of eight active cables driven from the base, fully controls the position, orientation, and grasping configuration of the device. This constitutes the first 7-DOF cable-driven robot that is made of a network of cables instead of a pure parallel architecture. Original static and kinematic models were developed to address the particularities of the proposed architecture. They are detailed in this manuscript and used to define the workspace and the control algorithm of the design. A working prototype illustrating an implementation of the theory is presented.**

I. INTRODUCTION

To provide realistic force feedback, impedance controlled haptic devices need to be lightweight, such that the inertia of the devices themselves does not disturb the rendered forces. Further, they need to be stiff, such that the device can mechanically present high-frequency content forces. To improve the realism of force feedback in haptic devices, an increasing number of haptic devices are nowadays based on parallel robotic architectures. In a parallel haptic interface, the forces are transmitted from the base-located motors to the haptic end-effector, usually in the shape of a knob, using parallel closed-loop chains made of mechanical links and passive joints. Such architectures usually offer higher stiffness and lower inertia than their serial counterparts.

Cable-driven robots [1] are parallel robots in which cables connect the end-effector to motorised reels located on a base frame. They are generally lighter and with larger workspace than rigid parallel robots, which makes them good candidates for haptic devices, either in 3D planar [2], [3], 3D spatial [4], or in 5-DOF [5] and 6-DOF [6] workspace. Cable-driven haptic devices, however, generally do not provide grasping capabilities, which prevents natural interactions. It is indeed sometimes desirable to provide grasping force feedback via multiple contact points to allow the operator to feel the shape and stiffness of the manipulated objects. Limited research has been conducted on cable-driven robots that provide additional grasping. Either an external gripper is mounted at the top of an existing cable robot [7], [8] or a rigid platform is used to provide grasping [9], [10]. A planar cable platform was proposed in [11]. In this article, we propose a novel general purpose, lightweight haptic device based on a cable-driven robotic architecture that provides 1-DOF grasping in addition to full 6-DOF manipulation, using a configurable cable platform. The proposed device enables pinch grasping without using any mounted grasping motor or linkage made of rigid links and bearings. This is possible thanks to a configurable platform [12] made of passive cables kept in tension with which the operator interacts via the palm of the hand and the index and thumb fingers. The coordinated action of eight active cables fully controls the platform's position, orientation and grasping configuration while keeping all cables in tension. This article presents the first-ever spatial cable-driven robot made of a network of cables in tension, which required a design in which less independent static equations are present than the number of active and passive cables. The developed procedure could be easily generalised to more complex cable platforms with more internal DOFs. The next section describes the proposed architecture, while Sec. III presents the kinematic model that needed to be developed for the control of the device. Section IV presents the kinematic design and key properties of the resulting workspace while Sec. V shows the implementation of a working prototype that serves as concept validation.

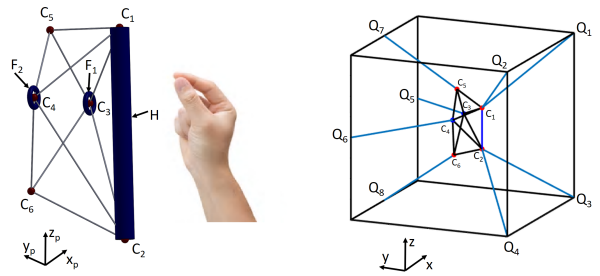

Fig. 1. Structure of the 7-DOF cable-driven robotic haptic device with a configurable cable platform. The operator interacts with the device using the palm of the hand on H, and the index and thumb fingers on F_1 and F_2. Eight actuated cables Q_i, attached on six points, C_i, on the platform control its position, orientation and grasping configuration.

II. ARCHITECTURE DESCRIPTION AND ANALYSIS

This section introduces the main components of the proposed cable-driven haptic device and the notation used in

This work was supported by the National Institute for Health Research (Invention for Innovation, i4i; II-LB-0716-20002). The views expressed are those of the author(s) and not necessarily those of the NHS, the National Institute for Health Research or the Department of Health and Social Care.

L. Da Cruz is with Wellcome/EPSRC Centre on Interventional and Surgical Sciences, University College London, UK and Moorfields Eye Hospital, London, UK. P. Lambert and C. Bergeles are with the School of Biomedical Engineering & Imaging Sciences, Faculty of Life Science and Medicine, King's College London, UK. Correspondence: patrice.lambert@kcl.ac.uk

This paper has supplementary video available at https: //ieeexplore.ieee.org, provided by the authors.

* denotes equal contribution.

this article, as well as a formal analysis of the mobility of the configurable platform. This platform constitutes the main innovation of this device and is made of ten passive cables kept in tension. It allows the operator to use the palm of the hand as well as the index and thumb finger to interact in 7-DOF with the device, including via pinch grasping.

A. Structure and Notation

The structure of the device is presented in Fig. 1. The operator interacts with the device using the palm of their hand on rigid body H, and the index and thumb fingers on F_1 and F_2. H, F_1 and F_2 are connected by a network of ten passive cables kept in tension by eight independent parallel active cables Q_i.

Assuming that all passive cables are kept in tension, the cable platform can be considered as an open polyhedron made of six rigid triangular faces, with one open boundary formed by the cables connecting vertices C_3, C_4, C_5, and C_6. The lengths of the passive cables are such that the platform is symmetric with respect to its local plane Y_pZ_p (illustrated in Fig. 1), which includes the long axis $S_h = \overleftrightarrow{C_1C_2}$ of handle (H) and the point at mid-distance between F_1 and F_2. The handle H is connected to four active cables via the connection points C_1 and C_2, while the four remaining attachment points are connected to one active cable each, for a total of eight active cables. The distance between F_1 and F_2 can vary to change the configuration of the platform, providing the grasping capability.

Arguably, a platform with the same structure made of rigid elements instead of passive cables would lead to the same mobility and would provide rigid connections between the connection points C_i. However, in addition to being heavier and generating friction, rigid connections in this structure would present major impracticability. Specifically, the rigid system would be constructed with rigid rods replacing the passive cables, in which case 3-DOF spherical joints allowing multiple connections at the C_i location would be needed; this is challenging to implement in a simple or compact way. The system could also be constructed with six rigid plates corresponding to the six triangular faces, connected by ten 1-DOF hinges corresponding the passive cables, in which case the plates would collide with the operator's hand.

Cable-driven parallel robots require at least one more cable than the number of DOFs to keep all cables in tension without the help of an external force. We will now show that the platform possess indeed 1 configurable DOF in addition to the 6-DOF of conventional cable-driven robots and therefore operates with the minimum number of active cables possible.

B. Mobility Analysis

Assuming all cables are kept in tension, for mathematical purposes the configurable platform can be considered as six triangular plates connected by seven 1-DOF revolute hinges. As shown in Fig. 2, the topology graph results in a parallel mechanism with three kinematic chains between plates P_3

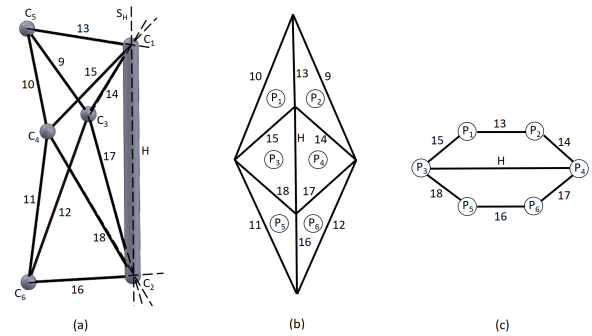

Fig. 2. Mobility analysis of the configurable platform. The numbers denoting the cables are consistent throughout (a), (b), and (c). (a) Illustration of the platform assuming that the ten passive cables are kept in tension. (b) The configurable platform mobility is equivalent to a mechanism with six triangular plates connected by seven 1-DOF revolute joints. (c) Topology graph showing that the platform constitutes a parallel mechanism with three kinematic chains.

and P_4. If $\boldsymbol{\xi_i}$ is the unit twist screw of virtual revolute joint i, the twist system of mobility of the mechanism T_m is

$$T_m = \boldsymbol{\xi_H} \cap \left(\sum_{i=13}^{15} \boldsymbol{\xi_i} \right) \cap \left(\sum_{i=16}^{18} \boldsymbol{\xi_i} \right) = \boldsymbol{\xi_H} \qquad (1)$$

where $\boldsymbol{\xi_H}$ corresponds to a 1-DOF rotation around the axis S_H of the handle, $T_u = \Sigma_{i=13}^{15} \xi_i$ is the mobility of the upper chain in Fig. 2(c) and $T_l = \Sigma_{i=16}^{18} \xi_i$ is the mobility of the lower chain. Indeed, since both screw systems T_u and T_l consist of a 3-DOF system with three virtual joints having their axes of revolution intersecting on a single point on the axis S_H, they can both emulate any rotation around their respective intersection point, including rotation $\boldsymbol{\xi_H}$. Furthermore, the three base screw vectors in both T_u and T_l are linearly independent, meaning that no additional mobility is included in their kinematic chain.

It can also be noted that $\boldsymbol{\xi_H}$ applies five independent constraints between P_3 and P_4, while systems T_u and T_l each apply three overconstraints in translation between those virtual plates. Applying the modified Chebychev mobility criteria [13] with $n = 6$ bodies, $j = 7$ joints and $r = 6$ over-constraints, the mobility M is given by

$$M = 6\,(n-1) - 5j + r = 30 - 35 + 6 = 1\,, \qquad (2)$$

confirming that the platform has indeed 1-DOF.

In the next section, the kinematics and statics of the device are developed. Our analysis show how the device can provide a range of force-feedback in any given configuration within the workspace, while ensuring all cables are kept in tension.

III. Kinematics and Statics

For a conventional 6-DOF cable-driven device with m active cables, the inverse position kinematics is easily determined from the distance between the cable attachment points on the platform and the base, and its statics is based on a structural matrix $\mathbf{A^T}$ of dimension $6 \times m$, where each column is formed by the wrench screw vector of an active cable. In the proposed architecture, due to the presence of the configurable cable platform with its network of cables

and multiple bodies, additional steps are needed to calculate the inverse position kinematics and statics.

First, we define the position of the end-effectors $\mathbf{p}$ and actuators $\mathbf{q}$ with vectors of dimension 7, and 8, respectively:

$$\mathbf{p} = \begin{bmatrix} x & y & z & \theta_x & \theta_y & \theta_z & \rho \end{bmatrix}^T \quad (3)$$

$$\mathbf{q} = \begin{bmatrix} q_1 & q_2 & q_3 & q_4 & q_5 & q_6 & q_7 & q_8 \end{bmatrix}^T , \quad (4)$$

where x, y, and z correspond to the position at the centre of the handle while θ_x, θ_y, and θ_z are the axial components of rotation vector $\boldsymbol{\theta}$ around the centre position. Variable ρ corresponds to the half of the angle that is formed between finger 1 (F_1), the handle (H), and finger 2 (F_2). The length of actuated cable i, with $i = 1, \ldots, 8$ is represented by q_i.

Similarly, two additional vectors are used to describe the static forces in the end-effector and actuator domains:

$$\mathbf{f} = \begin{bmatrix} f_x & f_y & f_z & \tau_x & \tau_y & \tau_z & \tau_\rho \end{bmatrix}^T \quad (5)$$

$$\mathbf{t_a} = \begin{bmatrix} t_1 & t_2 & t_3 & t_4 & t_5 & t_6 & t_7 & t_8 \end{bmatrix}^T , \quad (6)$$

where f_x, f_y, f_z are the three components of the force, and τ_x, τ_y, τ_z are the three components of the moment applied on the end-effector. Variable τ_ρ represents the moment applied between the two fingers (F_1) and (F_2) around the axis S_h of the handle (H). This is the force counterpart of the angular variable ρ, such that $\tau_\rho \times \rho$ corresponds to the grasping power delivered to the system. Finally, vector $\mathbf{t}$ contains the tensions of the eight actuated cables. Since we used the rotation vector convention for the orientation we can easily calculate the power transmitted to the device as $\mathbf{f} \cdot \dot{\mathbf{p}} = \boldsymbol{\tau_a} \cdot \dot{\mathbf{q}}_\mathbf{i}$. As the five rigid components of the platform are lightweight and speed is generally slow in haptic applications, all elements are considered mass-less and infinitely stiff. Therefore dynamic effects are not considered critical in this instance for the impedance control of the robot, but are still relevant from a design point of view in particular with the frequency content of the force feedback.

A. Inverse Position Kinematics

This section establishes the non-linear mapping from the end-effector position, $\mathbf{p}$, onto the length of the actuated cables, $\mathbf{q}$. The challenge is primarily found in the determination of the 3D location of the six cable attachment points, *i.e.* C_i on the platform, since the length of an actuated cable simply corresponds to the distance between its attachment points on the base and platform. The ten passive cables forming the configurable cable platform do not change in length, and their position/orientation in space can also be fully defined from the six attachment points. Since the grasping configuration of the 1-DOF platform is fully defined by the grasping value ρ, the first step is to express the position of the platform attachment points in the local frame of the platform, which has its origin located at the middle of the handle (H), as a function of ρ. The first two attachment points, $\mathbf{c_{p1}}$ and $\mathbf{c_{p2}}$, are fixed on the handle and are therefore independent of ρ. Contrary, $\mathbf{c_{p3}}$ and $\mathbf{c_{p4}}$ are directly located on the fingertip effectors and their position in the local frame is dependent on ρ. We have

$$\mathbf{c_{p1}} = \begin{bmatrix} 0 & 0 & h \end{bmatrix}^T \qquad \mathbf{c_{p2}} = \begin{bmatrix} 0 & 0 & -h \end{bmatrix}^T$$

$$\mathbf{c_{p3}} = \begin{bmatrix} m\sin(\rho) \\ m\cos(\rho) \\ g-h \end{bmatrix} \qquad \mathbf{c_{p4}} = \begin{bmatrix} -m\sin(\rho) \\ m\cos(\rho) \\ g-h \end{bmatrix} \quad (7)$$

where h is half the length of the handle H, $g = \left(l_{17}^2 + (2h)^2 - l_{14}^2\right) / (4h)$ is the Z_p-component of the vector from $\mathbf{c_{p2}}$ to $\mathbf{c_{p3}}$ or $\mathbf{c_{p4}}$, and $m = \sqrt{l_{17}^2 - g^2}$ is the shortest distance between $\mathbf{c_{p3}}$ or $\mathbf{c_{p4}}$ and the handle H, with $l_{17} = l_{18}$ and $l_{14} = l_{15}$ being the lengths of the cables connecting the fingers to the handle. Because of the platform symmetry in its local Y_pZ_p plane, attachment points $\mathbf{c_{p5}}$ and $\mathbf{c_{p6}}$ lie on it. Specifically, they are located at the intersection of a circle in the Y_pZ_p plane that is centred on the corresponding handle attachment point, and a sphere centred on a finger effector attachment point. Therefore, their closure equations, *i.e.* the conditions needed to close the mechanical loops, can be expressed as:

$$\left|\left|\mathbf{c_p} - l_h \begin{bmatrix} 0 & \cos(\phi) & \sin(\phi) \end{bmatrix}^T\right|\right|^2 = l_f^2 . \quad (8)$$

Depending whether the position of C_5 or C_6 is computed, ϕ is the angle between the Y_p axis and either cable 13 or 16. Further, $\mathbf{c_p}$ corresponds to either $(\mathbf{c_{p3}} - \mathbf{c_{p1}})$ or $(\mathbf{c_{p3}} - \mathbf{c_{p2}})$, l_h is either l_{13} or l_{16}, and l_f is either l_{10} or l_{11}. Due to the symmetry of the platform, identical results would be obtained by using $\mathbf{c_{p5}}$ instead of $\mathbf{c_{p3}}$. Developing (8), we obtain

$$c_{py}\cos(\phi) + c_{pz}\sin(\phi) = \frac{|\boldsymbol{c_p}|^2 + l_h^2 - l_f^2}{2l_f} . \quad (9)$$

Finally, using the tangent half-angle substitution in (9), ϕ is

$$\phi = 2\tan^{-1}\left(\frac{c_{pz} \pm \sqrt{c_{pz}^2 + c_{py}^2 - w^2}}{w + c_{py}}\right) , \quad (10)$$

where $w = \left(|\boldsymbol{c_p}|^2 + l_h^2 - l_f^2\right)/2l_h$. The $\pm$ represents the two solutions in a sphere-circle intersection; the positive sign must be selected for ϕ_{13}, while the negative sign is used for ϕ_{16}. The remaining platform attachment points are

$$\mathbf{c}_{p5} = \mathbf{c}_{p1} + l_{13}\begin{bmatrix} 0 & \cos(\phi_{13}) & \sin(\phi_{13}) \end{bmatrix}^T \quad (11)$$

$$\mathbf{c}_{p6} = \mathbf{c}_{p1} + l_{16}\begin{bmatrix} 0 & \cos(\phi_{16}) & \sin(\phi_{16}) \end{bmatrix}^T . \quad (12)$$

With the positions of the platform attachment points $\mathbf{c_{pi}}$ in the platform reference (X_p, Y_p, Z_p) frame known, their position $\mathbf{c_i}$ in the global reference frame is calculated as

$$\mathbf{c_i} = \mathbf{R}(\boldsymbol{\theta})\,\mathbf{c_{pi}} + \begin{bmatrix} x & y & z \end{bmatrix}^T , \quad (13)$$

where the rotation matrix $\mathbf{R}(\boldsymbol{\theta})$ is computed from the rotation vector $\boldsymbol{\theta} = \begin{bmatrix} \theta_x & \theta_y & \theta_z \end{bmatrix}^T$.

Using the positions $\mathbf{c_i}$ of the six platform attachment points C_i and the position of the eight actuators Q_j on the

base frame, the length and direction of all cables can be calculated, which is the inverse position kinematics.

B. Statics

In conventional cable-driven parallel robots, the static matrix $\mathbf{A^T}$ describes the linear relations between the forces $\mathbf{t_a}$ applied by the actuated cables and the resulting forces/moments $\mathbf{f}$ on the end-effector, such that $\mathbf{A^T t_a} = \mathbf{f}$. This equation is used to determine how much tension to apply on the actuated cables. However, in the case of this 7-DOF cable-driven robot, we must ensure that the passive cables are also kept in tension. The statics relation $\mathbf{A^T}$ in our case is expressed as:

$$\mathbf{A^T t}_{(18\times1)} = \mathbf{A^T} \begin{bmatrix} \mathbf{t_{a(8\times1)}} \\ \mathbf{t_{p(10\times1)}} \end{bmatrix} = \begin{bmatrix} \mathbf{f_{(7\times1)}} \\ \mathbf{0} \end{bmatrix}, \qquad (14)$$

where $\boldsymbol{t_p} = \begin{bmatrix} t_9 & \cdots & t_{18} \end{bmatrix}^T$ contains the passive cable tensions, and the zero vector $\mathbf{0}$ corresponds to the statics equilibrium equations not directly contributing to the forces $\mathbf{f}$ felt by the operator.

The linear relation is globally valid as long as the elements in $\mathbf{A^T}$ are updated as the device's configuration changes. Unlike conventional cable-driven parallel devices, our device has five rigid bodies instead of one: the handle H and fingers F_1 and F_2, which provide force-feedback to the operator, and the upper and bottom attachment points C_5 and C_6, which only serve to transmit forces between cables. The handle can be considered as a rigid body with 6-DOF while the four remaining bodies are point-objects with 3-DOF. Each body is affected not only by the tensions of the actuated cables $\boldsymbol{t_a}$ and by the operator forces $\boldsymbol{f}$, but also from the tension $\mathbf{t_p}$ in the passive cables of the configurable platform.

In a static configuration, the sum of forces and moments (six equations) acting on the handle (one item) must be zero; for point-objects (four items), only the sum of forces (three equations) is considered. This results in $1 \times 6 + 4 \times 3 = 18$ equations of force/moment equilibrium. Each set of three equations of forces is in the form $\sum \hat{\mathbf{d}}_\mathbf{i} t_i = \mathbf{f_j}$, where $\hat{\mathbf{d}}_\mathbf{i}$ corresponds to a unit vector in the direction of cable i and oriented away from the body j on which the cable is attached to. The tension in the cable i is t_i, and the vector $\mathbf{f_j}$ is the sum of forces on the body j, which will be $\mathbf{0}$ in case of body C_5 and C_6, and will correspond to the forces felt and compensated by the operator for F_1, F_2, and H.

The handle has only two cable attachment points, C_1 and C_2, located at equal distance h for its centre. Assuming that the operator exerts moments around the central point of the handle, the sum of moments on the handle from C_1 can be computed as $\sum \left(\hat{\mathbf{d}}_\mathbf{i} \times \mathbf{h}\right) t_i$, where $\mathbf{h}$ is a vector from the handle attachment point C_1 to the centre of the handle. Similarly, the sum of moments on the handle from C_2 can be computed as $\sum \left(\hat{\mathbf{d}}_\mathbf{i} \times (-\mathbf{h})\right) t_i$.

Combining the force and moment equations leads to a system of 18 equations with 18 unknown tensions t_i, where eight are actively controlled while ten are passive. Together, they are represented by the vector $\mathbf{t} = \begin{bmatrix} \mathbf{t_a}^T & \mathbf{t_p}^T \end{bmatrix}^T$. These

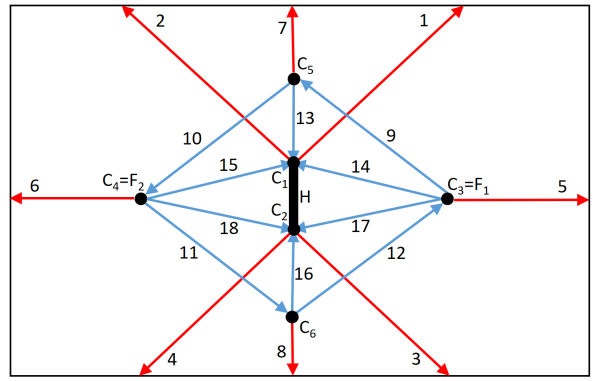

Fig. 3. Directed Graph representation of the network of cables with cables numbering. Cables in red are driven by actuators, while cables in blue are passive. For each cable i, there is a corresponding unit vector $\hat{\mathbf{d}}_\mathbf{i}$ directed along the cable. The orientation of this vector is arbitrary and is represented by an arrow on the cable. The six cable attachment points on the platform are denoted C_i, with C_1 and C_2 located on the handle H, and C_3, and C_4, located on the fingers F_1, and F_2, respectively.

equations can be assembled into a matrix system using the directed Graph presented in Fig. 3 to establish the attachment points of cables. The direction of the graph edges determines the sign of $\hat{\mathbf{d}}_\mathbf{i}$. The resulting matrix system is of the form

$$\mathbf{A^T_{so}}_{(18\times18)} \mathbf{t}_{(18\times1)} = \mathbf{f_{bo}}_{(18\times1)} \qquad (15)$$

where

$$\mathbf{A^T_{so}} = \begin{bmatrix} \hat{\mathbf{d}}_1 & \hat{\mathbf{d}}_2 & \hat{\mathbf{d}}_3 & \hat{\mathbf{d}}_4 & 0 & 0 & 0 & 0 & 0 & 0 & 0 & 0 & -\hat{\mathbf{d}}_{13} & -\hat{\mathbf{d}}_{14} & -\hat{\mathbf{d}}_{15} & -\hat{\mathbf{d}}_{16} & -\hat{\mathbf{d}}_{17} & -\hat{\mathbf{d}}_{18} \\ \hat{\mathbf{d}}_1 \times \hat{\mathbf{h}} & \hat{\mathbf{d}}_2 \times \hat{\mathbf{h}} & -\hat{\mathbf{d}}_3 \times \hat{\mathbf{h}} & -\hat{\mathbf{d}}_4 \times \hat{\mathbf{h}} & 0 & 0 & 0 & 0 & 0 & 0 & 0 & 0 & -\hat{\mathbf{d}}_{13} \times \hat{\mathbf{h}} & -\hat{\mathbf{d}}_{14} \times \hat{\mathbf{h}} & -\hat{\mathbf{d}}_{15} \times \hat{\mathbf{h}} & \hat{\mathbf{d}}_{16} \times \hat{\mathbf{h}} & \hat{\mathbf{d}}_{17} \times \hat{\mathbf{h}} & \hat{\mathbf{d}}_{18} \times \hat{\mathbf{h}} \\ 0 & 0 & 0 & 0 & \hat{\mathbf{d}}_5 & 0 & 0 & 0 & \hat{\mathbf{d}}_9 & 0 & 0 & -\hat{\mathbf{d}}_{12} & 0 & \hat{\mathbf{d}}_{14} & 0 & 0 & \hat{\mathbf{d}}_{17} & 0 \\ 0 & 0 & 0 & 0 & 0 & \hat{\mathbf{d}}_6 & 0 & 0 & 0 & -\hat{\mathbf{d}}_{10} & \hat{\mathbf{d}}_{11} & 0 & 0 & 0 & \hat{\mathbf{d}}_{15} & 0 & 0 & \hat{\mathbf{d}}_{18} \\ 0 & 0 & 0 & 0 & 0 & 0 & \hat{\mathbf{d}}_7 & 0 & -\hat{\mathbf{d}}_9 & \hat{\mathbf{d}}_{10} & 0 & 0 & \hat{\mathbf{d}}_{13} & 0 & 0 & 0 & 0 & 0 \\ 0 & 0 & 0 & 0 & 0 & 0 & 0 & \hat{\mathbf{d}}_8 & 0 & 0 & -\hat{\mathbf{d}}_{11} & \hat{\mathbf{d}}_{12} & 0 & 0 & 0 & \hat{\mathbf{d}}_{16} & 0 & 0 \end{bmatrix}$$

and

$$\mathbf{f_{bo}} = \begin{bmatrix} \mathbf{f_H}^T & \boldsymbol{\tau}_\mathbf{H}^T & \mathbf{f_{C3}}^T & \mathbf{f_{C4}}^T & \mathbf{f_{C5}}^T & \mathbf{f_{C6}}^T \end{bmatrix}^T \qquad (16)$$

with $\hat{\mathbf{h}}$ being a unit vector directed from the center of the handle to C_1. Each vector present in $\mathbf{A^T_{so}}$ and $\mathbf{f_{bo}}$ is of dimension (3×1). Since cables can only act in tension, the vector $\mathbf{t}$ can only contain positive elements, which is an unlikely solution for a system with the same number of equations as unknowns, as is (15). However, since the handle has only two attachment points, C_1 and C_2, the cables cannot apply any moment around the handle central axis S_h (which links C_1 and C_2). Moments around this axis can still be provided to the operator via linear forces on the fingers F_1 and F_2. Since all the cables attached to the handle intersect with S_h, no moment can be applied around this axis and only two out of the $4, 5, 6$-th rows in $\mathbf{A^T_{so}}$ are independent, making the 18×18 matrix $\mathbf{A^T_{so}}$ of rank 17. Therefore the solution $\mathbf{t}$ is not unique and a solution in which all elements are positive is possible.

This is an important aspect of the design, as cable-driven parallel robots indeed need at least one more cable

than the number of equations required to define their static equilibrium, since cables can only act in tension and not in compression. In order to create a system of 17 independent equations and change the structure of $\mathbf{A_{so}^T}$ according to its rank, we first apply the rotation matrix $-\mathbf{R}(\boldsymbol{\theta})$, corresponding to the inverse of the orientation of the platform, to rows 4 to 6 of (15). Row 6 of the resulting static matrix now corresponds to the moments around S_h (the Z axis in the local platform frame) and can be deleted, since all its elements are 0, to form the new matrix $\mathbf{A_s^T}$ and new vector $\mathbf{f_b}$. Mathematically, we can multiply both sides of (15) with

$$\mathbf{R_h} = \begin{bmatrix} \mathbf{I}_{(3\times3)} & \mathbf{0}_{(3\times3)} & \mathbf{0}_{(3\times12)} \\ \mathbf{0}_{(2\times3)} & -\mathbf{R_{1|2}}_{(2\times3)} & \mathbf{0}_{(2\times12)} \\ \mathbf{0}_{(12\times3)} & \mathbf{0}_{(12\times3)} & \mathbf{I}_{(12\times12)} \end{bmatrix}_{(17\times18)} \tag{17}$$

where $\mathbf{R_{1|2}}_{(2\times3)}$ is the first two rows of $\mathbf{R}$. We get

$$\begin{aligned} \mathbf{A_s^T} &= \mathbf{R_h}\mathbf{A_{so}^T}, \\ \mathbf{f_b} = \mathbf{R_h}\mathbf{f_{bo}} &= \left[\mathbf{f_h}^T \ \tau_1 \ \tau_2 \ \mathbf{f_{C3}}^T \ \mathbf{f_{C4}}^T \ \mathbf{f_{C5}}^T \ \mathbf{f_{C6}}^T\right]^T \end{aligned} \tag{18}$$

in which τ_1 and τ_2 are moments around the X_p and Y_p axes attached to local handle coordinate frame. Finally:

$$\mathbf{A_s^T}_{(17\times18)}\mathbf{t}_{(18\times1)} = \mathbf{f_b}_{(17\times1)} \tag{19}$$

In this static analysis, $\mathbf{f_b}$ represents the forces on the five bodies of the platform. To apply the desired force-feedback to the operator, we are only interested in the 7-DOF forces forming $\mathbf{f}$ in (5), which constitutes the input of the static problem. As explained above, the finger end-effectors F_1 and F_2 are used not only to provide grasping force-feedback when they generate forces in opposite directions, but also moment around the handle axis S_H when they generate forces in the same direction. To isolate the finger forces that contribute to the forces felt by the operator from the other forces distributed to the platform, we create a local reference frame for each finger F_i, formed by three perpendicular unit vectors $\mathbf{g_{ij}}$, where $\mathbf{g_{i3}}$ is a vector from F_i to the closest point on the handle axis S_h and perpendicular to it, $\mathbf{g_{i2}}$ has the same direction as the handle axis, and $\mathbf{g_{i1}} = \mathbf{g_{i3}} \times \mathbf{g_{i2}}$ corresponds to the mobility of F_i relative to the handle.

With m being the constant distance between the handle axis S_h and either F_1 or F_2, we have the following relations:

$$m\left(\mathbf{g_{11}^T}\mathbf{f_{C3}} + \mathbf{g_{21}^T}\mathbf{f_{C4}}\right) = \tau_3 \quad m\left(\mathbf{g_{21}^T}\mathbf{f_{C4}} - \mathbf{g_{11}^T}\mathbf{f_{C3}}\right) = \tau_\rho \tag{20}$$

where τ_3 is the moment around the Z axis of the handle and τ_ρ is the grasping moment. Both τ_3 and τ_p are exclusively provided by forces on F_1 and F_2. The remaining forces on F_1 and F_2 in static equilibrium must be 0. Therefore

$$\mathbf{g_{12}^T}\mathbf{f_{C3}} = \mathbf{g_{13}^T}\mathbf{f_{C3}} = \mathbf{g_{22}^T}\mathbf{f_{C4}} = \mathbf{g_{23}^T}\mathbf{f_{C4}} = 0\,. \tag{21}$$

Now that the relation between $\mathbf{f_h}$, τ_1, τ_2, τ_3,τ_ρ and the tension in the 18 cables $\mathbf{t}$ is known, (19) can be written as:

$$\mathbf{A^T t} = \mathbf{R}_\tau \mathbf{H}\mathbf{A_s^T}\mathbf{t}_{(18\times1)} = \mathbf{R}_\tau \mathbf{H}\mathbf{f_b} = \begin{bmatrix} \mathbf{f}_{(7\times1)} \\ \mathbf{0}_{(10\times1)} \end{bmatrix} \tag{22}$$

with

$$\mathbf{H} = \begin{bmatrix} \mathbf{I}_{(5\times5)} & \mathbf{0}_{(5\times6)} & \mathbf{0}_{(5\times6)} \\ \mathbf{0}_{(6\times5)} & \begin{matrix} m\hat{\mathbf{g}}_{11}^{\mathbf{T}} & m\hat{\mathbf{g}}_{21}^{\mathbf{T}} \\ m\hat{\mathbf{g}}_{11}^{\mathbf{T}} & -m\hat{\mathbf{g}}_{21}^{\mathbf{T}} \\ \hat{\mathbf{g}}_{12}^{\mathbf{T}} & \mathbf{0}_{(1\times3)} \\ \hat{\mathbf{g}}_{13}^{\mathbf{T}} & \mathbf{0}_{(1\times3)} \\ \mathbf{0}_{(1\times3)} & \hat{\mathbf{g}}_{22}^{\mathbf{T}} \\ \mathbf{0}_{(1\times3)} & \hat{\mathbf{g}}_{23}^{\mathbf{T}} \end{matrix} & \mathbf{0}_{(6\times6)} \\ \mathbf{0}_{(6\times5)} & \mathbf{0}_{(6\times6)} & \mathbf{I}_{(6\times6)} \end{bmatrix} \tag{23}$$

and

$$\mathbf{R}_\tau = \begin{bmatrix} \mathbf{I}_{(3\times3)} & \mathbf{0}_{(3\times3)} & \mathbf{0}_{(3\times11)} \\ \mathbf{0}_{(3\times3)} & \mathbf{R}_{(3\times3)}^{-1} & \mathbf{0}_{(3\times11)} \\ \mathbf{0}_{(11\times3)} & \mathbf{0}_{(11\times3)} & \mathbf{I}_{(11\times11)} \end{bmatrix} \tag{24}$$

(22) is the governing equation of the statics, and will be used to find the tensions in both active and passive cables, such that a 7-DOF force feedback $\mathbf{f}$ can be presented to the operator. It was shown in this section that the finger attachment points were selected to provide grasping and rotation around the handle axis (2-DOF), while the handle is used to provide the remaining 5-DOF.

It is worthwhile to mention that by selecting the forces in (21) to be 0, we ensure that the index and thumb fingers, being the only rigid elements connecting H with F_1 and F_2, are not used to transmit forces. It would have been indeed possible to consider the operator's hand as a rigid body, allowing forces to be applied on either H, F_1, or F_2 to increase the range of solutions for $\mathbf{t}$, but this would cause reaction forces on the fingers that could distract the operator from the desired force-feedback.

In order to obtain the vector of eight actuated cable tensions $\mathbf{t_a}$, included in $\mathbf{t}$, from the desired force-feedback $\mathbf{f}$ in a given position $\mathbf{p}$, one must solve the system of 17 equations and 18 unknowns in (22). This problem has an infinite number of solutions and we are interested in a solution that would minimise the norm of the tension vector while ensuring that all cables are kept in tension. Since the structural matrix $\mathbf{A^T}$ is of dimension 17×18, its null space is of dimension 1. If the device is in a configuration where static equilibrium can be reached while all cables are kept in tension, all elements of the eigenvector $\mathbf{t_0}$ in $\mathbf{A^T t_0} = \mathbf{0}$ will be of the same sign. As shown in [14], a particular solution $\mathbf{t_p} = \mathbf{A^T}^{+}\mathbf{f}$ can be obtained using the Moore-Penrose pseudoinverse and the complete set of solution is then given by $\mathbf{t_p} + \lambda\mathbf{t_0}$. Given a minimum tension t_{min} to prevent cable sagging, the optimal solution is obtained as:

$$\begin{cases} \mathbf{t} &= \mathbf{t_p} + \lambda\mathbf{t_0} \\ \lambda &= \max\limits_{i=1\ldots18} \dfrac{t_{min} - t_{pi}}{t_{0i}} \end{cases} \tag{25}$$

This λ value ensures that one element of $\mathbf{t}$ is equal to t_{min} while all the other elements are higher. In our prototype, the tensions t_{min} is set to 0.5 N to prevent sagging and t_{max} is 50 N for safety. If one element t_i is higher than an upper tension bound t_{max}, $\mathbf{f}$ must be scaled down until $t_{min} \leq t_i \leq t_{max}$ for all elements i.

C. Velocity Kinematics and Direct Position Kinematics

Direct position kinematics refers to finding the position vector $\mathbf{p}$ of the platform as function of the length of the eight active cables $\mathbf{q}$. This is the opposite of the problem presented in Sec. III-A, and is needed for determination of the device's configuration given cable sensors located at its base. Unlike the inverse position kinematics, direct kinematics generally do not have analytical solutions for parallel robots [15], thus numerical solutions are calculated.

First, we find the inverse velocity kinematics using (22) and the principle of power conservation. Assuming no friction, the only source and sink for power in the system come from the motors and the operator's interaction with the handle. Due to the presence of passive cables in the platform, we first need to decompose matrix $\mathbf{A^T}$ from (22) as:

$$\begin{bmatrix} \mathbf{A^T_{11}}_{(7\times 8)} & \mathbf{A^T_{12}}_{(7\times 10)} \\ \mathbf{A^T_{21}}_{(10\times 8)} & \mathbf{A^T_{22}}_{(10\times 10)} \end{bmatrix} \begin{bmatrix} \mathbf{t_a} \\ \mathbf{t_p} \end{bmatrix} = \begin{bmatrix} \mathbf{f} \\ \mathbf{0} \end{bmatrix} \tag{26}$$

from which the direct relation between $\mathbf{t_a}$ and $\mathbf{f}$ is:

$$\mathbf{A^T_p}_{(7\times 8)} \mathbf{t_a} = \left(\mathbf{A^T_{11}} - \mathbf{A^T_{12}} \mathbf{A^{-T}_{22}} \mathbf{A^T_{21}}\right) \mathbf{t_a} = \mathbf{f} \tag{27}$$

While (27) is more compact than (22), it cannot be used in practice for statics since it cannot ensure that the passive cables $\mathbf{t_p}$ are kept in tension. It can however be used to derive the relation between forces and velocities in the actuator and effector spaces. When power is conserved, we have:

$$\begin{gathered} -\mathbf{t_a}^T \dot{\mathbf{q}} = \mathbf{f}^T \dot{\mathbf{p}} = \left(\mathbf{A^T_p} \mathbf{t_a}\right)^T \dot{\mathbf{p}} = \mathbf{t_a}^T \mathbf{A_p} \dot{\mathbf{p}} \\ \dot{\mathbf{q}} = -\mathbf{A_p} \dot{\mathbf{p}} \end{gathered} \tag{28}$$

The negative sign in $-\mathbf{t_a}^T \dot{\mathbf{q}}$ comes from the fact that power is given to the system when moment and velocity in a motor are in the same direction, which is the case when the cable lengths diminish since cables are always kept in tension. The Moore-Penrose pseudo-inverse $(+)$ can be used for the direct velocity kinematic such as $\dot{\mathbf{p}} = -\left(\mathbf{A_p}\right)^+ \dot{\mathbf{q}}$. Since $\mathbf{A_p}$ is a rectangular matrix, not every vector $\dot{\mathbf{q}}$ is permitted in (28). If a not permitted input $\dot{\mathbf{q}}$ is used as input for the direct velocity kinematics, as is the case in practice due to calibration errors, the pseudo inverse will find the vector $\dot{\mathbf{p}}$ corresponding to the closest permitted vector $\dot{\mathbf{q}}$.

Finally, the following Gauss-Newton algorithm is used to solve the direct position kinematics:

$$\begin{aligned} \boldsymbol{q}_k &= g_{IPK}\left(\mathbf{p}_k\right) \\ \Delta \boldsymbol{q} &= \boldsymbol{q}_{sensors} - \boldsymbol{q}_k \\ \Delta \boldsymbol{p} &= -\left(\mathbf{A_p}\right)^+ \Delta \boldsymbol{q} \\ \boldsymbol{p}_{k+1} &= \boldsymbol{p}_k + \Delta \boldsymbol{p} \end{aligned} \tag{29}$$

where g_{IPK} corresponds to the inverse position kinematic problem described in Sec. III-A, and $\mathbf{p}_k$ is initially an estimate of the device position. The process repeats until the results of successive iterations change less than the desired resolution. Although Gauss-Newton algorithm (GNA) is sometimes complemented with gradient descent in a Levenberg-Marquardt algorithm (LMA) for robustness, GNA was sufficient for convergence in our case. Results not included for brevity showed speed advantages in using GNA over LMA without sacrifice in accuracy.

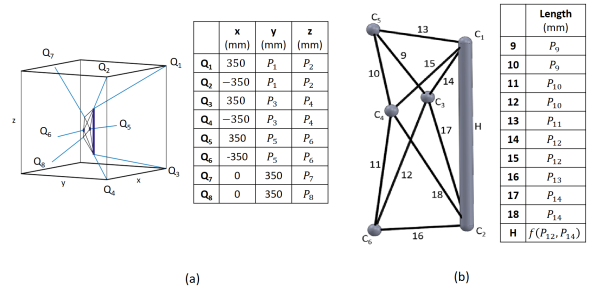

	x (mm)	y (mm)	z (mm)
Q_1	350	P_1	P_2
Q_2	−350	P_1	P_2
Q_3	350	P_3	P_4
Q_4	−350	P_3	P_4
Q_5	350	P_5	P_6
Q_6	-350	P_5	P_6
Q_7	0	350	P_7
Q_8	0	350	P_8

	Length (mm)
9	P_9
10	P_9
11	P_{10}
12	P_{10}
13	P_{11}
14	P_{12}
15	P_{12}
16	P_{13}
17	P_{14}
18	P_{14}
H	$f(P_{12}, P_{14})$

Fig. 4. List of the 14 design parameters; (a) 8 parameters are used to define cable attachment points (b) 6 parameters are used to define the platform passive cable length

IV. Kinematic Design

Once the kinematics and statics have been established for a general design, a set of design parameters can be selected for the implementation of the actual device. The first step is to list all the design parameters that have an influence on the kinematic and static relations described in the section above. Some of those parameters can be already fixed due to practical and ergonomic considerations. For example, the distance between the fingers and the palm of the hand resulting from the length of some of the passive cables can be based on the average length of fingers, and the base frame dimensions can be based on the available footprint and ergonomic reach of the human arm.

Let's first consider the dimensions of the base frame. From a kinematic point of view, there is generally no drawback in increasing the size of the base as it only results in larger workspace, more constant Jacobian matrix, and homogeneous performance. A larger frame also renders small deflections from the model, for example the actual point of contact with the pulley, negligible for the calculation of cable lengths. From a practical point of view, the main limitations are the footprint available and the reach of the human arm. We therefore selected the frame to be as large as possible within ergonomic comfort for a standing operator as 700×700 mm in the horizontal plane and 640 mm in height. The last kinematic parameter to be selected from ergonomic considerations is the constant distance g between the handle axis S_H and the finger interfaces F_1 and F_2, set at $g = 70$mm, which will act as a constraint on the remaining design parameters.

The set of design parameters is presented in Fig. 4. Thanks to the symmetry of the design in its YZ plane, the number of actual independent parameters can be reduced. There are two distinct sets of parameters; the positions on the frame where the cables are connected and reeled by a pulley system, and the lengths of the passive cables of the platform.

As the front side of the frame must be free to let the operator easily access to the 7-DOF haptic interface, Q_1, Q_3, and Q_5 are located on the right side of the frame, parallel to the YZ plane, while Q_2, Q_4, and Q_6 are located on the left side. Attachment points Q_7 and Q_8 are located on the back

panel. Using symmetry in the YZ plane to reduce the number of design parameters, we finally obtain eight parameters for the cable attachment points Q_i on the frame. For the cable platform, using symmetry in the YZ plane and the constraint imposed by the distance between the handle and the fingers, we can describe the lengths of the handle and the passive cables with 6 independent parameters. The length of the rigid handle (H) is calculated as:

$$f\left(P_{12}, P_{14}\right) = \sqrt{P_{12}^2 - g^2} + \sqrt{P_{14}^2 - g^2} \tag{30}$$

This set of 14 kinematic parameters is used in the design procedure to maximise the workspace. As it is generally the case in parallel robots, the total workspace is coupled in all dimensions, *i.e* that the boundaries in each dimension are dependent on the position in other dimensions. For haptic applications, it is not always possible or desirable for the operator to consider this coupling. We therefore use a sub-region of the total workspace, designated as the useful workspace, in which certain ranges of orientations $(\theta_x, \theta_y, \theta_z)$ and grasping values ρ are possible at any (x, y, z).

A configuration $\mathbf{p}$ is interior to the full workspace if a static equilibrium can be reached, which occurs as described in Sec. III-B when all the elements of the null vector $\mathbf{t_0}$ of matrix $\mathbf{A^T}$ are of the same sign. If a static equilibrium can be reached with $\mathbf{f} = \mathbf{0}$, then a solution to the cable tension $\mathbf{t}$ with all positive elements is possible for any force $\mathbf{f}$.

A position (x, y, z) is considered to be inside the useful workspace if it is inside the full workspace for all values of orientations and grasping within certain ranges. The four ranges used in this procedure are $[-15°, 15°]$ for orientations α, β, and γ, and $[20°, 35°]$ for the half-grasping value ρ. It is a fair assumption to consider that all configurations within a range are inside the workspace if both its upper and lower limits are in the workspace as well, *i.e.* that there is no void in the workspace. Each position is tested for all combinations of upper and lower limits of the four ranges, leading to $2^4 = 16$ configurations for each position.

In this procedure, a numerical approximation of the volume of the useful workspace is used as the objective function. Since the objective function is computed a large number of times during the process, it is important to select a fast-computing method and to consider what is an acceptable approximation of the volume. The volume of the useful workspace is calculated using the method of [16], which is briefly summarised below.

First, we define a regular octahedron with 8 triangular faces and 12 edges for which each of the 8 triangular faces is then divided into a set of sub-triangles up to a desired resolution. The vertices of these triangles form a set of points to which directional vectors $\mathbf{u}$ can be drawn from the center O of the workspace. These vectors are then multiplied by a scalar λ to correspond to the limit of the useful workspace, using the bisection method. Both the number of points in each face and the stopping criteria of the bisection method will influence the resolution of the workspace and the speed for its calculation. Once the magnitude is fixed, each triangle

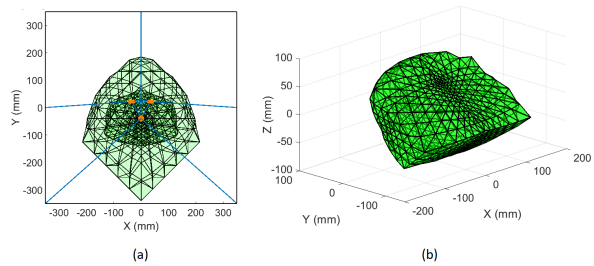

Fig. 5. (a) Translational workspace with Volume$(0°) = 1.74 \times 10^7$ mm^3 and useful workspace with Volume$(\pm 15°) = 3.65 \times 10^6$ mm^3 for $\rho = [20°, 35°]$ on the footprint of the robot. The center position is $[0, -40, -10]$ (b) 3D representation of the useful workspace

now represents a flat approximation for a region of the boundaries of the workspace, and a pyramidal volume can be created by connecting the three points of the triangle to the center of the workspace. For a volume represented by L triangles, each with three points A, B, and C, the volume V is calculated as

$$V = \frac{(\mathbf{u}_A \times \mathbf{u}_B) \cdot \mathbf{u}_C}{6} \sum^{L} \lambda_A \lambda_B \lambda_C \tag{31}$$

where the scalar triple product is the volume formula for a parallelepiped and has the same value for each triangle on the unit octahedron surface.

This volume is used as the objective function for the 14 design parameters P_i shown in Fig. 4. The cable attachment points $i = 1, ..., 8$ are constrained to remain in the limits of the frame surfaces and the length of the platform cables $i = 9, ..., 14$ are kept between 30 mm and 200 mm. In practice, since the cables are connected to a ring and only pointing at the virtual connection point, the lower limit is used to leave place to the rigid bodies of the platform and limit errors. The upper limit constraints the size ratio of the platform to the base frame. Since the objective function can present discontinuities and has multiple local minima, a genetic algorithm was used for the selection of those parameters. Genetic algorithms are search methods based on the principle of natural selection that are suitable for searching global minima without the use of gradient information. In addition, they generally perform well if the objective function is fast and the number of parameters is low. Although they do not guarantee optimal or repeatable results, they are useful in improving performance of initial designs. Final parameters are shown in Table I.

Using these parameters, Fig. 5(a) shows the translational workspace and the useful workspace for half grasping $\rho = [20°, 35°]$ in regard to the footprint of the device. The volume of the useful workspace with $\pm 15°$ for orientations α, β, and γ is s 3.652×10^6 mm^3 and its 3D representation is shown in Fig. 5(b). This corresponds to a subset of the full workspace for which the central boundaries are shown in Table II.

V. Prototype Implementation

A working prototype of the proposed architecture is shown in Fig. 6. An experiment was conducted with an operator

TABLE I

VALUES OF DESIGN PARAMETERS

Parameter	P_1	P_2	P_3	P_4	P_5	P_6	P_7
Value (mm)	-350	320	-350	-320	0	-60	320
Parameter	P_8	P_9	P_{10}	P_{11}	P_{12}	P_{13}	P_{14}
Value (mm)	-320	54	69	108	145	91	148

TABLE II

WORKSPACE CENTRAL BOUNDARIES

(mm or °)	x	y	z	θ_x	θ_y	θ_z	θ_ρ
max	188	208	148	29	23	26	68
min	-188	-309	-113	-24	-23	-26	10

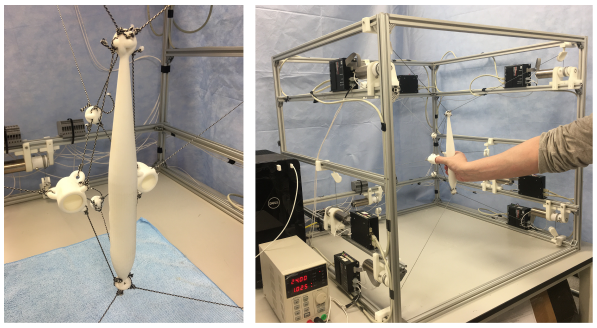

Fig. 6. Left: 3D printed platform for pinch grasping. Right: Prototype.

moving the device successively in each DOF, covering a large portion of the full workspace boundaries of Table II. The cable lengths are recorded from the motor encoders and the direct kinematic model (29) is used to calculate the platform position, orientation, and grasping configuration. At the same time, the position, orientation, and grasping configuration of the device is recorded with a NDI Aurora electromagnetic tracker to validate the direct position kinematics. Fig. 7(a) shows the calculated position (x, y, and z) using (29), and its comparison with the external electromagnetic tracker. Fig. 7(b) shows the equivalent for the orientation and grasping angles (α, β, γ, and ρ). Results show that the numerical procedure always converges and that the average error is 1.73 mm with a standard deviation of ± 1.59 mm for the position values, while an average error of $1.45°$ with a standard deviation of $0.95°$ is obtained for angular values. This is comparable to the human precision for reaching absolute positions in free air with visual feedback, which is about 1 mm. It should be noted that the numerical procedure for the direct kinematics involves the computation of the inverse position and velocity kinematic, as well as the computation of the structural matrix $\mathbf{A}^{\mathbf{T}}$ described in this article, validating these models.

VI. CONCLUSIONS

This article presented a novel 7-DOF cable-driven haptic device that provides pinch grasping capability using the introduced concept of a configurable cable platform, which is made of a network of cables in tension. This constitutes the first spatial cable-driven robots that is made of a network of cables instead of a pure parallel architecture. Its kinematic model was developed and validated with a working prototype. The concept of configurable cable platform can also be applied in other cable robot applications requiring grasping.

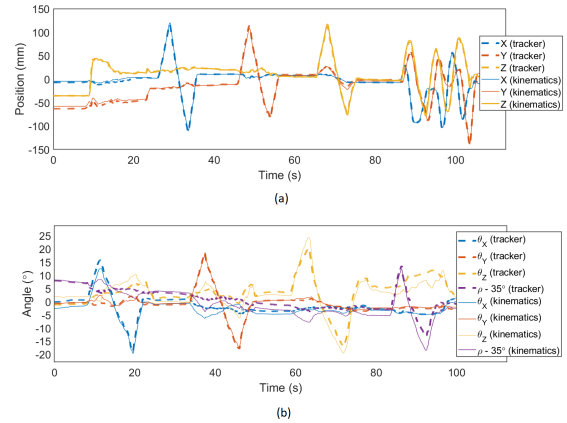

Fig. 7. Comparison of direct kinematics with ground truth from electromagnetic tracker for (a) position (x, y, and z), (b) orientation and grasping angles (α, β, γ, and ρ).

REFERENCES

[1] A. Pott, *Cable-driven parallel robots: theory and application*. Springer, 2018, vol. 120.

[2] C. Gosselin, R. Poulin, and D. Laurendeau, "A planar parallel 3-DOF cable-driven haptic interface," *World Multi-Conference on Systemics, Cybernetics and Informatics*, pp. 266–271, 2008.

[3] Y. Yang and Y. Zhang, "A new cable-driven haptic device for integrating kinesthetic and cutaneous display," *ASME/IFToMM Int. Conf. Reconfigurable Mechanisms and Robots*, pp. 386–391, 2009.

[4] J. Saint-Aubert, S. Régnier, and S. Haliyo, "Cable driven haptic interface for co-localized desktop VR," *IEEE Haptics Symposium*, pp. 351–356, 2018.

[5] G. Rosati, D. Zanotto, and A. Rossi, "Performance assessment of a 3D cable-driven haptic device," *ASME Int. Mechanical Engineering Congress and Exposition*, pp. 597–606, 2008.

[6] A. Fortin-Côté, P. Cardou, and C. Gosselin, "An admittance control scheme for haptic interfaces based on cable-driven parallel mechanisms," *IEEE Int. Conf. Robotics and Automation*, pp. 819–825, 2014.

[7] A. Pott, H. Mütherich, W. Kraus, V. Schmidt, P. Miermeister, and A. Verl, "IPAnema: a family of cable-driven parallel robots for industrial applications," in *Cable-Driven Parallel Robots*. Springer, 2013, pp. 119–134.

[8] T. Bruckmann, W. Lalo, K. Nguyen, and B. Salah, "Development of a storage retrieval machine for high racks using a wire robot," *ASME Int. Design Engineering Technical Conf. and Computers and Information in Engineering Conf.*, pp. 771–780, 2012.

[9] S. Kim, J. Berkley, and M. Sato, "A novel seven degree of freedom haptic device for engineering design," *Virtual Reality*, vol. 6, no. 4, pp. 217–228, 2003.

[10] A. Martin, S. Caro, and P. Cardou, "Design of a cable-driven parallel robot with grasping device," *Procedia CIRP*, vol. 70, pp. 290–295, 2018.

[11] K. S. Jadhao, P. Lambert, T. Bruckmann, and J. L. Herder, "Design and analysis of a novel cable-driven haptic master device for planar grasping," *Cable-Driven Parallel Robots*, pp. 307–318, 2018.

[12] P. Lambert and J. L. Herder, "Parallel robots with configurable platforms: Fundamental aspects of a new class of robotic architectures," *Proceedings of the Institution of Mechanical Engineers, Part C: Journal of Mechanical Engineering Science*, vol. 230, no. 3, pp. 463–472, 2016.

[13] J. M. McCarthy and G. S. Soh, *Geometric design of linkages*. Springer Science & Business Media, 2010, vol. 11.

[14] D. Zanotto, G. Rosati, S. Minto, and A. Rossi, "Sophia-3: A semiadaptive cable-driven rehabilitation device with a tilting working plane," *IEEE Trans. Robotics*, vol. 30, no. 4, pp. 974–979, 2014.

[15] M. L. Husty, "An algorithm for solving the direct kinematics of general stewart-gough platforms," *Mechanism and Machine Theory*, vol. 31, no. 4, pp. 365–379, 1996.

[16] A. Pott, "Forward kinematics and workspace determination of a wire robot for industrial applications," in *Advances in Robot Kinematics: Analysis and Design*. Springer, 2008, pp. 451–458.